SS1

Single-shot read-out of an individual electron spin in a quantum dot

J. M. Elzerman, R. Hanson, L. H. Willems van Beveren, B. Witkamp, L. M. K. Vandersypen & L. P. Kouwenhoven

Nature, 430, 431 (2004)

Magnetic field: $B > 8\,T$

Temperature: $T \simeq 0.25\,K$

Spin relaxation time: $T_1 \simeq 0.85\,ms$

Single-shot fidelity: 65 %

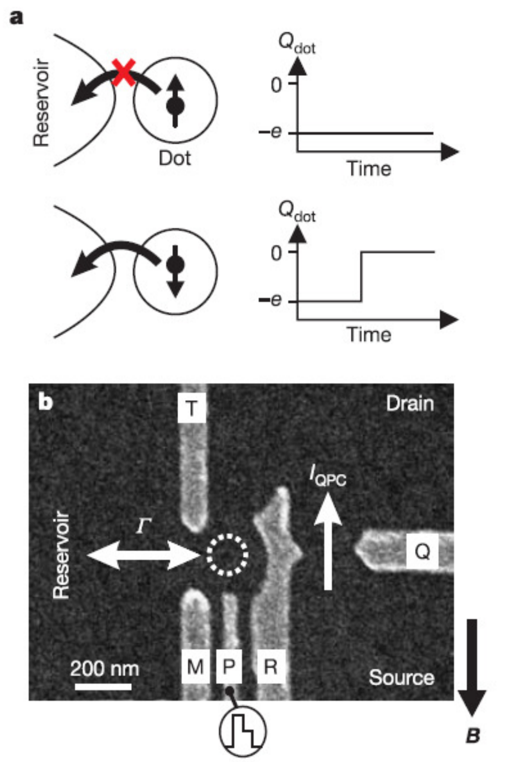

Figure 1 Spin-to-charge conversion in a quantum dot coupled to a quantum point contact. **a**, Principle of spin-to-charge conversion. The charge on the quantum dot, Q_{dot}, remains constant if the electron spin is ↑, whereas a spin-↓ electron can escape, thereby changing Q_{dot}. **b**, Scanning electron micrograph of a device like the one used in the measurements, showing the metallic gates (T, M, P, R, Q) on the surface of a GaAs/AlGaAs heterostructure containing a two-dimensional electron gas (2DEG) 90 nm below the surface. The electron density is $2.9 \times 10^{15}\,m^{-2}$. (Only the gates used in the present experiment are shown, the complete device[23] is described in Supplementary Fig. S1.) By measuring the current through the QPC channel, I_{QPC}, we can detect changes in Q_{dot} that result from electrons tunnelling between the dot and the reservoir (with a tunnel rate Γ). A magnetic field, B, is applied in the plane of the 2DEG.

SS2

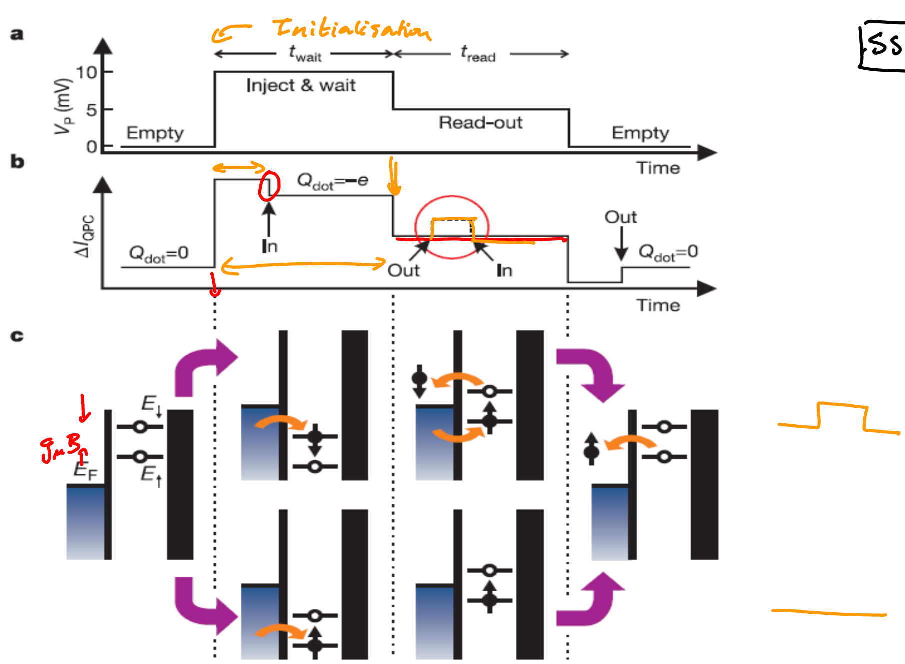

Figure 2 Two-level pulse technique used to inject a single electron and measure its spin orientation. **a**, Shape of the voltage pulse applied to gate P. The pulse level is 10 mV during t_{wait} and 5 mV during t_{read} (which is 0.5 ms for all measurements). **b**, Schematic QPC pulse-response if the injected electron has spin-↑ (solid line) or spin-↓ (dotted line; the difference with the solid line is only seen during the read-out stage). Arrows indicate the moment an electron tunnels into or out of the quantum dot. **c**, Schematic energy diagrams for spin-↑ ($E_\uparrow$) and spin-↓ ($E_\downarrow$) during the different stages of the pulse. Black vertical lines indicate the tunnel barriers. The tunnel rate between the dot and the QPC drain on the right is set to zero. The rate between the dot and the reservoir on the left is tuned to a specific value, Γ. If the spin is ↑ at the start of the read-out stage, no change in the charge on the dot occurs during t_{read}. In contrast, if the spin is ↓, the electron can escape and be replaced by a spin-↑ electron. This charge transition is detected in the QPC current (dotted line inside red circle in **b**).

SS3

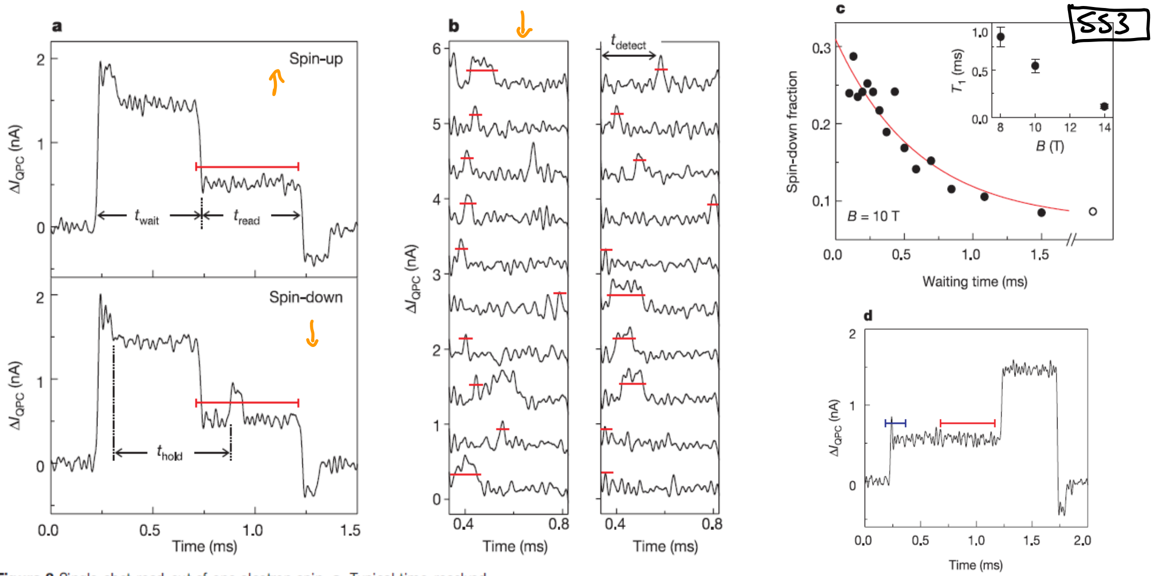

Figure 3 Single-shot read-out of one electron spin. **a**, Typical time-resolved measurements of the QPC current in response to a two-level pulse. In the top panel, an electron is injected during t_{wait} and is declared 'spin-up' during t_{read}. In the lower panel, the injected electron is declared 'spin-down' by the characteristic step which crosses the threshold (red line) during t_{read}. The total time the electron spends in the dot is defined as t_{hold}. **b**, Randomly chosen examples of traces for which the electron is declared 'spin-down' (here for the case of $t_{wait} = 0.1$ ms). Only the read-out segment is shown, and traces are offset for clarity. The actual time when ΔI_{QPC} first crosses the threshold (red line), t_{detect}, is recorded to make the histogram in Fig. 4a. **c**, Fraction of traces counted as spin-down versus waiting time, t_{wait}, out of a total of 625 traces taken for each waiting time. Rightmost point (open dot): spin-down fraction using modified pulse shape (**d**). Red solid line: exponential fit to the data. Inset: T_1 versus B (see Supplementary Fig. S4). Error bars represent the root mean square of the standard errors obtained from exponential fits to three separate data sets. **d**, Typical QPC signal for a 'reversed' pulse, which has the same amplitudes as in Fig. 2a, but with the order of the two stages reversed. In this case injection takes place with $E_{\uparrow}$ below and $E_{\downarrow}$ above E_F (see Fig. 2c, third column), so that only a spin-↑ electron can be injected. By recording the fraction of traces in which the current nevertheless crosses the threshold of duration t_{read} (red line), an independent measure of the 'dark count' probability is obtained (see text). This fraction is plotted as the open dot in **c**. It is used in the exponential fit with an associated value of $t_{wait} = 10$ ms (that is, much longer than the spin relaxation time). The blue threshold is used in Fig. 4b.

Coherent Manipulation of Coupled Electron Spins in Semiconductor Quantum Dots

Science, 309, 2180 (2005)

SS4

J. R. Petta,[1] A. C. Johnson,[1] J. M. Taylor,[1] E. A. Laird,[1] A. Yacoby,[2] M. D. Lukin,[1] C. M. Marcus,[1] M. P. Hanson,[3] A. C. Gossard[3]

(0,2)

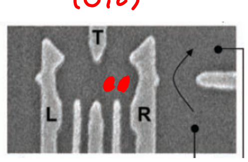

(1,1)

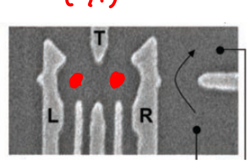

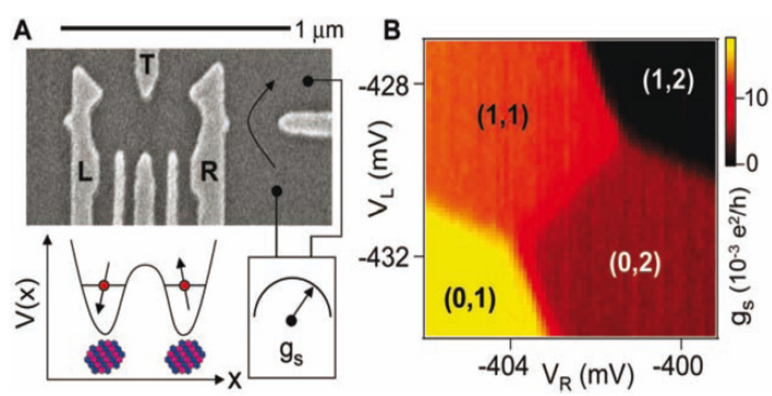

Fig. 1. (A) Scanning electron micrograph of a sample identical to the one measured, consisting of electrostatic gates on the surface of a two-dimensional electron gas. Voltages on gates L and R control the number of electrons in the left and right dots. Gate T is used to adjust the interdot tunnel coupling. The quantum point contact conductance g_s is sensitive primarily to the number of electrons in the right dot. (B) g_s measured as a function of V_L and V_R reflects the double-dot charge stability diagram (a background slope has been subtracted). Charge states are labeled (m,n), where m is the number of electrons in the left dot and n is the number of electrons in the right dot. Each charge state gives a distinct reading of g_s.

No tunneling, $B=0$:

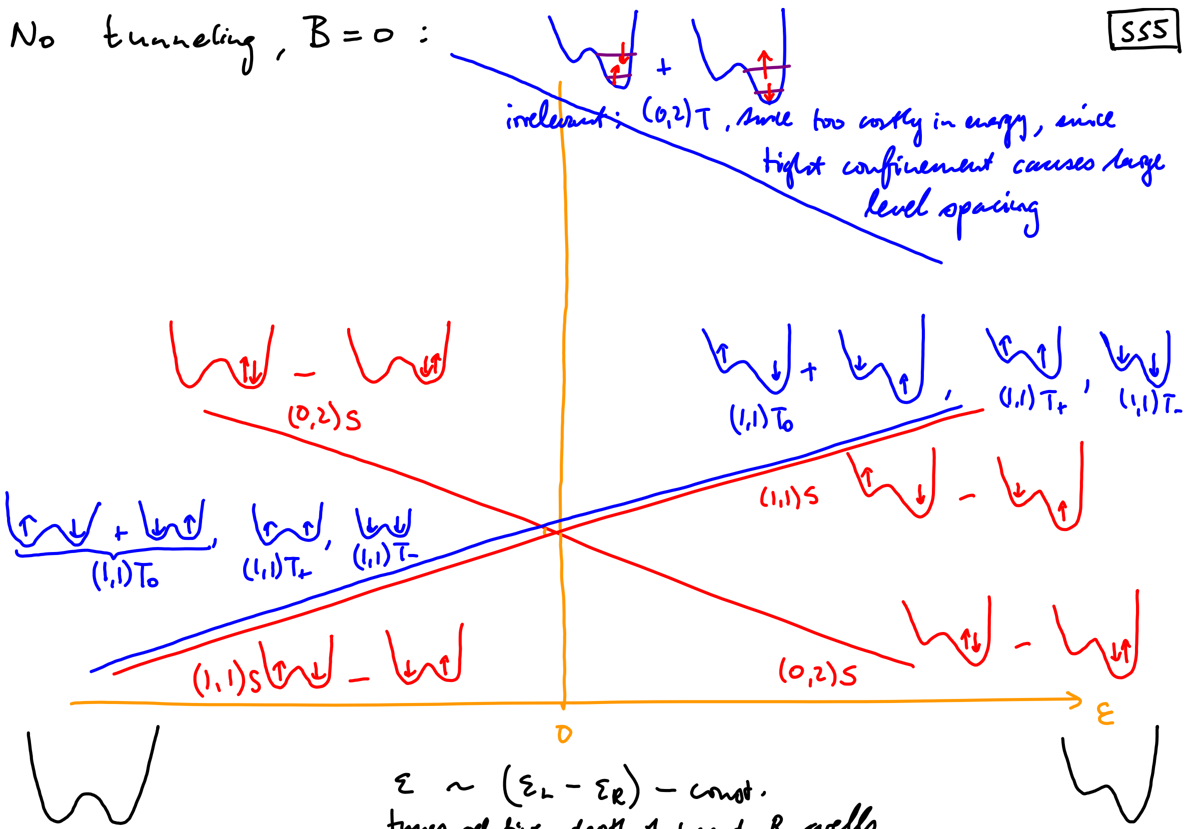

$\varepsilon \sim (\varepsilon_L - \varepsilon_R)$ − const. times relative depth of L and R wells

SS6

: $(0,2)S = |0\rangle_L \otimes \left(|\uparrow,\downarrow\rangle_R - |\downarrow,\uparrow\rangle_R\right)/\sqrt{2} = c^\dagger_{R\uparrow} c^\dagger_{R\downarrow}|0\rangle$

"joined singlet state"

: $(1,1)S = \frac{1}{\sqrt{2}}\left(|\uparrow\rangle_L |\downarrow\rangle_R - |\downarrow\rangle_L |\uparrow\rangle_R\right)$

"separated singlet state"

$= \frac{1}{\sqrt{2}}\left(c^\dagger_{L\uparrow} c^\dagger_{R\downarrow} \mp c^\dagger_{L\downarrow} c^\dagger_{R\uparrow}\right)|0\rangle$

: $(1,1)T_0 = \frac{1}{\sqrt{2}}\left(|\uparrow\rangle_L |\downarrow\rangle_R + |\downarrow\rangle_L |\uparrow\rangle_R\right)$

(1,1)T_+ : $(1,1)T_+ = |\uparrow\rangle_L \otimes |\uparrow\rangle_R = c^\dagger_{L\uparrow} c^\dagger_{R\uparrow}|0\rangle$

(1,1)T_- : $(1,1)T_- = |\downarrow\rangle_L \otimes |\downarrow\rangle_R = c^\dagger_{L\downarrow} c^\dagger_{R\downarrow}|0\rangle$

Effect of tunneling $(1,1) \Leftrightarrow (0,2)$

With tunneling: $\quad |\sigma\rangle_L |\sigma'\rangle_R \xleftrightarrow[\text{(no spin flip)}]{\text{tunneling}} \begin{cases} |0\rangle_L |\sigma,\sigma'\rangle_R & \text{if } \sigma' = -\sigma \\ 0 & \text{if } \sigma' = \sigma \end{cases}$ (1)

$$H_{\text{tunnel}} \, |(1,1)T_{\bar\sigma}\rangle = \sum_\sigma \left(c^\dagger_{R\sigma} c_{L\sigma}\right) c^\dagger_{L\bar\sigma} c^\dagger_{R\bar\sigma} |0\rangle = c^\dagger_{R\bar\sigma} c^\dagger_{R\bar\sigma} |0\rangle = 0 \tag{2}$$

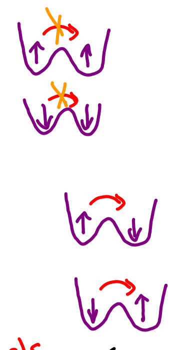

$$H_{\text{tunnel}} \begin{Bmatrix} |(1,1)T_0\rangle \\ |(1,1)S\rangle \end{Bmatrix} = \sum_\sigma \left(c^\dagger_{R\sigma} c_{L\sigma}\right) \frac{1}{\sqrt2}\left(c^\dagger_{L\uparrow} c^\dagger_{R\downarrow} \pm c^\dagger_{L\downarrow} c^\dagger_{R\uparrow}\right)|0\rangle \tag{3}$$

$$= \frac{1}{\sqrt2}\left(c^\dagger_{R\uparrow} c^\dagger_{R\downarrow} \pm c^\dagger_{R\downarrow} c^\dagger_{R\uparrow}\right)|0\rangle = \begin{cases} 0 \leftarrow \{c^\dagger_\uparrow, c^\dagger_\downarrow\} = 0. \\ \sqrt2 \, c^\dagger_{R\uparrow} c^\dagger_{R\downarrow}|0\rangle = \sqrt2 \, (0,2)S \end{cases} \tag{4}$$

$$\Rightarrow \quad \langle (1,1)S \,|\, H_{\text{tunnel}} \,|\, (0,2)S\rangle \neq 0 \qquad \langle (1,1)T \,|\, H_{\text{tunnel}} \,|\, (0,2)S\rangle = 0 \tag{5}$$

Within subspace of $|(1,1)S\rangle$, $|(0,2)S\rangle$: $\quad H_{\text{eff}} = \frac12 \begin{pmatrix} \varepsilon & T(\varepsilon) \\ T(\varepsilon) & -\varepsilon \end{pmatrix} \Rightarrow$ splitting: $E_\pm = \frac12\sqrt{\varepsilon^2 + T^2(\varepsilon)}$ (6)

$J(\varepsilon) = \varepsilon - E_-$

With tunneling, $B \neq 0$:

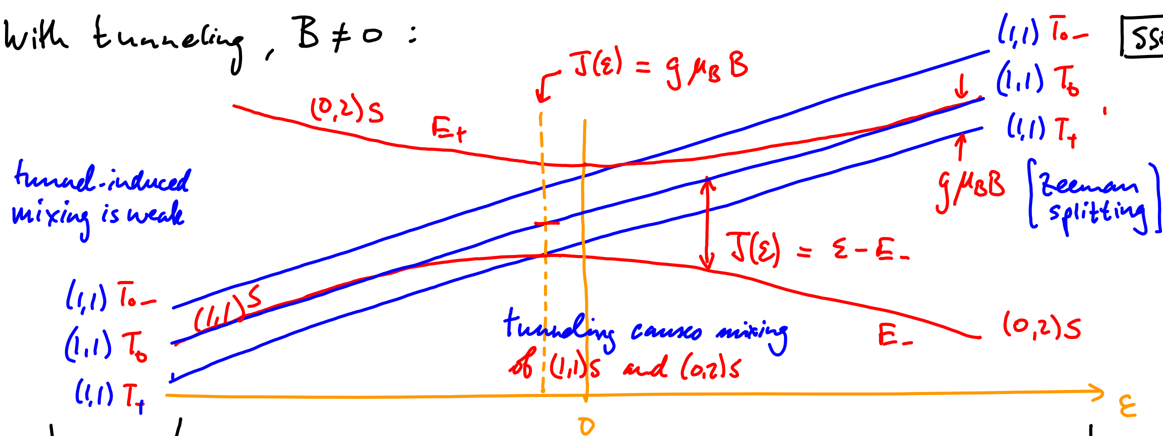

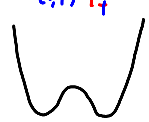

$\varepsilon \sim (\varepsilon_L - \varepsilon_R)$ – const.
times relative depth of L and R wells

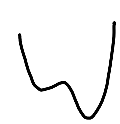

Splitting between $(1,1)T_0$ and $(1,1)S$: $J(\varepsilon)$

At large negative detuning, where $J(\varepsilon) \ll 0$:

$|0\rangle \equiv (1,1)S = \frac{1}{\sqrt2}\left(|\uparrow\rangle_L|\downarrow\rangle_R - |\downarrow\rangle_L|\uparrow\rangle_R\right)$ north pole

$|1\rangle \equiv (1,1)T_0 = \frac{1}{\sqrt2}\left(|\uparrow\rangle_L|\downarrow\rangle_R - |\downarrow\rangle_L|\uparrow\rangle_R\right)$ south pole

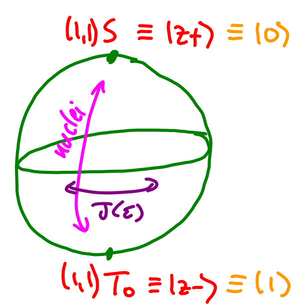

55a

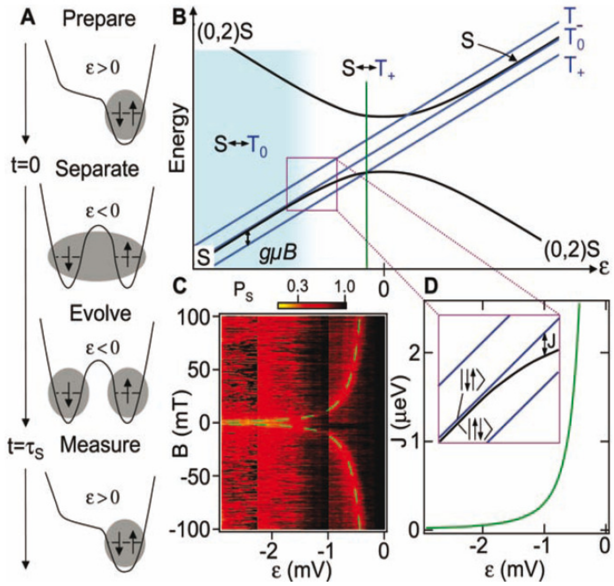

Fig. 2. (A) The control cycle for experiments generally consists of preparation, singlet separation, evolution of various kinds, and projection onto the (0,2) singlet state (measurement). Projective measurement is based on the spin-blockaded transition of T states onto (0,2)S, whereas S states proceed freely, allowing S to be distinguished from T by the charge sensor during the measurement step. (B) Energy diagram near the (1,1)-to-(0,2) charge transition. A magnetic field splits T states by the Zeeman energy. At the S-T_0 degeneracy (light blue region) and the S-T_+ degeneracy (green line), hyperfine fields drive evolution between S and the respective T states. (C) Singlet probability P_S after τ_s = 200 ns, as a function of detuning ε and magnetic field B maps out degeneracies of S-T_0 ($\varepsilon < \sim -1.2$ mV) and S-T_+ (dashed green curve). (D) Dependence of exchange on detuning, extracted from the fit of $J(\varepsilon) = g^*\mu_B B$ along the S-T_+ resonance, assuming $g^* = -0.44$ [dashed curve in (C)]. (Inset) For $J(\varepsilon) \gg g^*\mu_B B_{nuc}$, eigenstates S and T_0 are split by $J(\varepsilon)$. At large negative detuning, $J(\varepsilon) \ll g^*\mu_B B_{nuc}$, and S and T_0 are mixed by hyperfine fields but eigenstates $|\uparrow\downarrow\rangle$ and $|\downarrow\uparrow\rangle$ are not.

$(1,1)S = \frac{1}{\sqrt{2}}\left(|\uparrow\rangle_L|\downarrow\rangle_R - |\downarrow\rangle_L|\uparrow\rangle_R\right)$

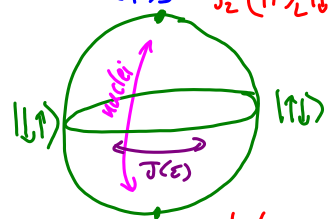

$(1,1)T_0 = \frac{1}{\sqrt{2}}\left(|\uparrow\rangle_L|\downarrow\rangle_R - |\downarrow\rangle_L|\uparrow\rangle_R\right)$

Initialize & readout:

via $(0,2)S$

Manipulate:

via $|\uparrow\downarrow\rangle \overset{J(\varepsilon)}{\longleftrightarrow} |\downarrow\uparrow\rangle$

and $|S\rangle \overset{\text{nuclear spins}}{\longleftrightarrow} |T_0\rangle$

55b

Readout: Quickly sweep back from $\varepsilon < 0$ to $\varepsilon > 0$.

$(1,1)S$ will be converted by tunneling to $(0,2)S$, detected by QPC.

$(1,1)T$ has zero tunnel matrix element with $(0,2)S$,

because they have different spin symmetry

So, repeating experiment N times, detector will show $(0,2)S$

$N \cdot P_S$ times, where P_S = probability that $(1,1)$ is found in $(1,1)_T$

In general: $P_S = P_S(\varepsilon, B)$

Manipulation: Hyperfine interaction with nuclear spins $\boxed{SS11}$

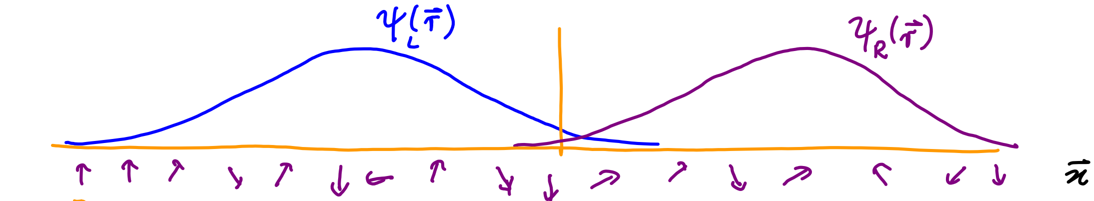

Randomly-pointing nuclear spins $\quad \sim |\psi(x_j)|^2 \quad x_j$ = site of nucleus j

$$H_{\text{electron-nuclei}} = \underbrace{\sum_{j=\text{all nuclei}} \bar{J}_j \, \vec{S}_j}_{\vec{B}_{\text{nucl}}} \cdot \vec{S}_0$$

$\vec{S}_j$: nuclear spins ($S = 3/2$); $\vec{S}_0$: electron spin

"hyperfine field" $\quad \vec{B}_{\text{nucl}} \sim 1$ to 5 mT, direction is random!

Nuclear spins evolve slowly, on scale of $> 10\ \mu s$ > manipulation time ($\sim$ few μs)

$\Rightarrow$ Nuclear field "looks static", but mixes all $(1,1)T_{0,+,-}, S$ states

Qubit Hamiltonian: for $J(\varepsilon) \ll g^* \mu_B B$ $\boxed{SS12}$

and $B \gg B_{\text{nuc}}$ $\quad$ (to split off $(1,1)T_{\pm}$ from $(1,1)T_0$):

Consider subspace

$$|S\rangle \equiv (1,1)S = \tfrac{1}{\sqrt{2}}\left(|\uparrow\rangle_L|\downarrow\rangle_R - |\downarrow\rangle_L|\uparrow\rangle_R\right) \equiv |z+\rangle$$

$$|T\rangle \equiv (1,1)T_0 = \tfrac{1}{\sqrt{2}}\left(\underbrace{|\uparrow\rangle_L|\downarrow\rangle_R}_{\equiv|\uparrow\downarrow\rangle} - \underbrace{|\downarrow\rangle_L|\uparrow\rangle_R}_{|\downarrow\uparrow\rangle}\right) \equiv |z-\rangle$$

eigenstates of H_{el-nuc}
energy difference: ΔB^z_{nuc}

Here, $|\sigma\rangle_L|\sigma'_R\rangle$ are "instantaneous" eigenstates of $H_{\text{electron-nuclei}}$, i.e. quantization axis in left and right dot can be different: $\hat{z}_L \neq \hat{z}_R$

$$H_{\text{qubit}} = \begin{pmatrix} -J(\varepsilon) & \Delta B^z_{\text{nuc}} \\ \Delta B^z_{\text{nuc}} & 0 \end{pmatrix}$$

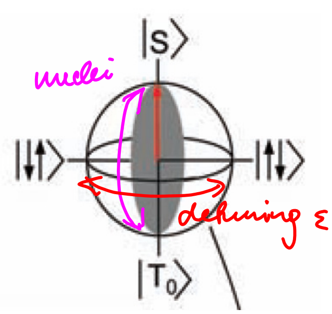

Measurement of $J(\varepsilon)$

SS13

nuclear spins mix $|S\rangle$ and $|T_0\rangle$ and $|T_+\rangle$ and $|T_-\rangle$, if energetically accessible: $\Big\{$ if $E((1,1)S) = E((1,1)T_+)$, i.e. if $J(\varepsilon) = g\mu_B B$

causing a reduction in $P_S(\varepsilon, B)$

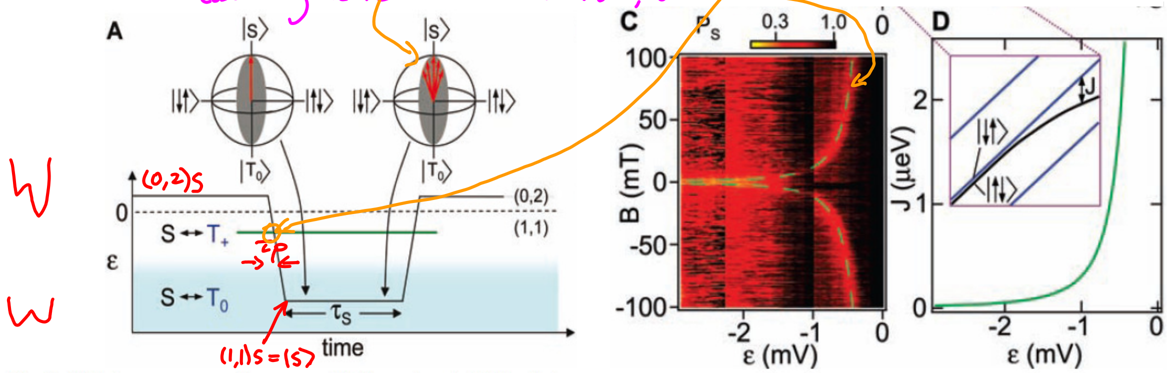

Fig. 3. (A) Pulse sequence used to measure T_2^*. The system is initialized into (0,2)S and transferred by rapid adiabatic passage to the spatially separated S state. With $T_\pm$ separated by a Zeeman field, S and T_0 mix at large detuning (light blue region), where hyperfine fields drive rotations about the x axis in the Bloch sphere. After a separation time τ_S, the state is projected onto (0,2)S. ~~drive evolution between S and the respective T states.~~ (C) Singlet probability P_S after τ_S = 200 ns, as a function of detuning ε and magnetic field B maps out degeneracies of S-T_0 (ε < ~ −1.2 mV) and S-T_+ (dashed green curve). (D) Dependence of exchange on detuning, extracted from the fit of $J(\varepsilon) = g^*\mu_B B$ along the S-T_+ resonance, assuming $g^* = -0.44$ [dashed curve in (C)]. (Inset) For $J(\varepsilon) \gg g^*\mu_B B_{nuc}$, eigenstates S and T_0 are split by $J(\varepsilon)$. At large negative detuning, $J(\varepsilon) \ll g^*\mu_B B_{nuc}$, and S and T_0 are mixed by hyperfine fields but eigenstates $|\uparrow\downarrow\rangle$ and $|\downarrow\uparrow\rangle$ are not.

rapid adiabatic passage: sweep time ($\tau_P \simeq 1\,\mu s$) is slow compared to tunnel time ($\tau_P \ll \hbar / J(0)$) fast compared to nuclear mixing time ($\tau_P \gg \frac{\hbar}{g\mu_B B_{nuc}}$)

Measurement of dephasing time T^* of (1,1)S

SS14

nuclear spins cause dephasing

direction and strength of nuclear field, and hence amount of precession, change from one run to the next

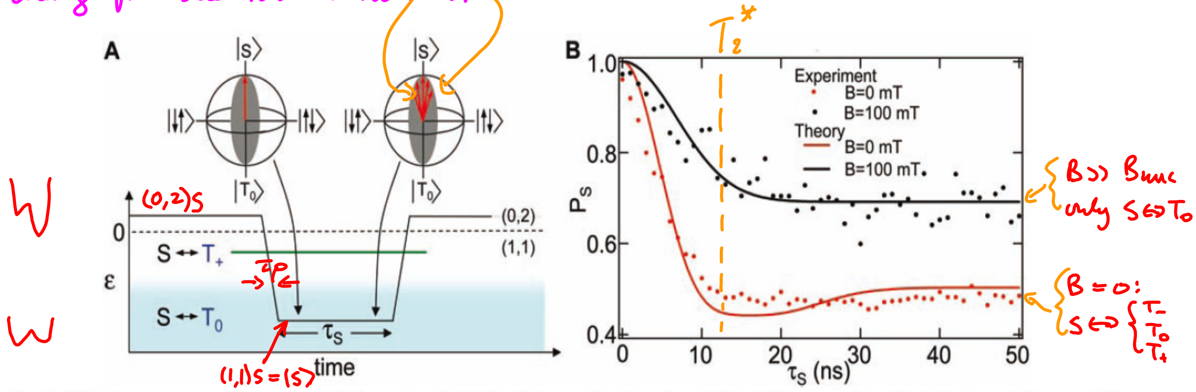

Fig. 3. (A) Pulse sequence used to measure T_2^*. The system is initialized into (0,2)S and transferred by rapid adiabatic passage to the spatially separated S state. With $T_\pm$ separated by a Zeeman field, S and T_0 mix at large detuning (light blue region), where hyperfine fields drive rotations about the x axis in the Bloch sphere. After a separation time τ_S, the state is projected onto (0,2)S. (B) Singlet probability P_S measured using the calibrated QPC charge sensor, as a function of τ_S at 100 mT (black curve) and 0 mT (red curve). For $\tau_S \ll T_2^*$, the singlet state does not have ample time to dephase, and $P_S \sim 1$. For $\tau_S \gg T_2^*$, $P_S \sim 0.7$ at 100 mT and $P_S \sim 0.5$ at 0 mT. A semiclassical model of dephasing due to hyperfine coupling (23) predicts $P_S \sim 1/2$ at high field and $P_S \sim 1/3$ at zero field. Fits to the model (solid curves), including a parameter adjusting measurement contrast, give $T_2^* = 10$ ns and $B_{nuc} = 2.3$ mT.

rapid adiabatic passage: sweep time ($\tau_P \simeq 1\,\mu s$) is slow compared to tunnel time ($\tau_P \ll \hbar / J(0)$) fast compared to nuclear mixing time ($\tau_P \gg \frac{\hbar}{g\mu_B B_{nuc}}$)

S15

Rabi oscillations in $|\uparrow\downarrow\rangle$, $|\downarrow\uparrow\rangle$ basis

Adiabatic in/out:

$\tau_A \gg T_2^*$, so superpositions decay

$(|\uparrow\downarrow\rangle \pm |\downarrow\uparrow\rangle)/\sqrt{2}$

$\rightarrow |\uparrow\downarrow\rangle$

Manipulation: suddenly switch on

$J(\varepsilon) \neq 0$, for a time

$T_2^* \gtrsim \tau_E \gg \frac{\hbar}{g\mu_B B}$

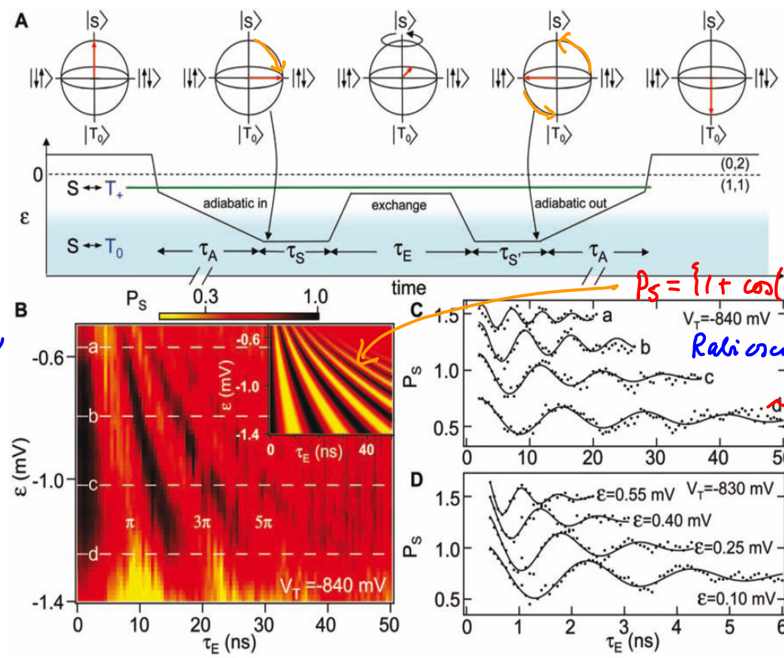

$P_S = \{1 + \cos(J(\varepsilon)\tau_E/\hbar)\}$

Rabi oscillation period $1/J(\varepsilon)$

faster oscillations for $\varepsilon > 0$, larger $J(\varepsilon)$

Fig. 4. (A) Pulse sequence demonstrating exchange control. After initializing into (0,2)S, detuning ε is swept adiabatically with respect to tunnel coupling through the S-T_+ resonance (quickly relative to S-T_+ mixing), followed by a slow ramp (τ_A ~ 1 μs) to large detuning, loading the system in the ground state of the nuclear fields $|\uparrow\downarrow\rangle$. An exchange pulse of duration τ_E rotates the system about the z axis in the Bloch sphere from $|\uparrow\downarrow\rangle$ to $|\downarrow\uparrow\rangle$. Reversing the slow adiabatic passage allows the projection onto (0,2)S to distinguish states $|\uparrow\downarrow\rangle$ and $|\downarrow\uparrow\rangle$ after time τ_E. Typically, $\tau_S = \tau_S' = 50$ ns. (B) P_S as a function of detuning and τ_E. The z-axis rotation angle $\phi = J(\varepsilon)\tau_E/\hbar$ results in oscillations in P_S as a function of both ε and τ_E. (Inset) Model of P_S using $J(\varepsilon)$ extracted from S-T_+ resonance condition, assuming $g^* = -0.44$ and ideal measurement contrast (from 0 to 1). (C) Rabi oscillations measured in P_S at four values of detuning indicated by the dashed lines in (B). Fits to an exponentially damped cosine function, with amplitude, phase, and decay time as free parameters (solid curves), are shown. Curves are offset by 0.3 for clarity. (D) Faster Rabi oscillations are obtained by increasing tunnel coupling and by increasing detuning to positive values, resulting in a π-pulse time of ~350 ps.

S16

Spin-echo

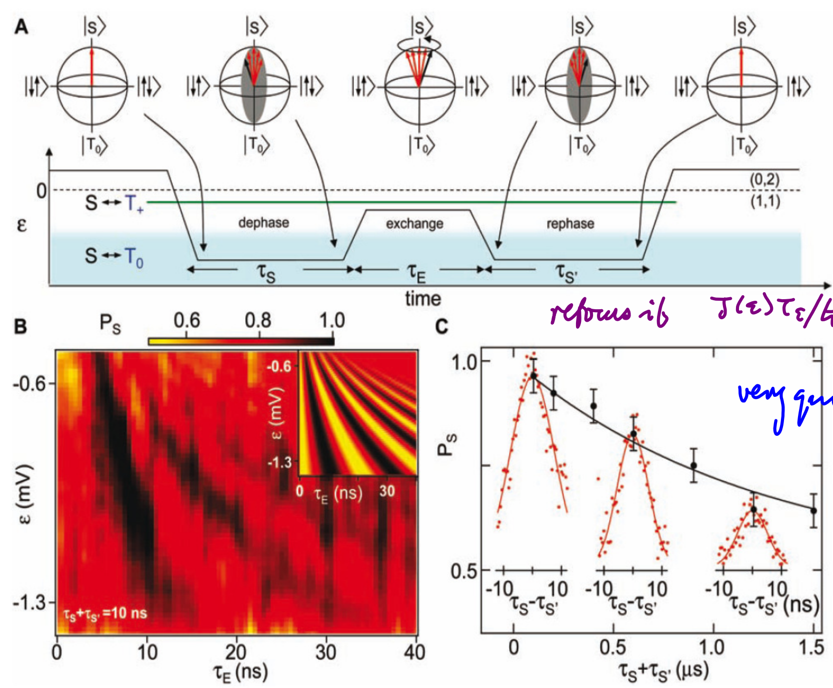

refocus if $J(\varepsilon)\tau_E/\hbar = \pi, 3\pi, 5\pi$

very quick decay if $\tau_S \neq \tau_S'$

Fig. 5. (A) Spin-echo pulse sequence. The system is initialized in (0,2)S and transferred to S by rapid adiabatic passage. After a time τ_S at large negative detuning, S has dephased into a mixture of S and T_0 due to hyperfine interactions. A z-axis π pulse is performed by making detuning less negative, moving to a region with sizable $J(\varepsilon)$ for a time τ_E. Pulsing back to negative detunings for a time $\tau_S' = \tau_S$ refocuses the spin singlet. (B) P_S as a function of detuning and τ_E. The z-axis rotation angle $\phi = J(\varepsilon)\tau_E/\hbar$ results in oscillations in P_S as a function of both ε and τ_E. (Inset) Model of P_S using $J(\varepsilon)$ extracted from the S-T_+ resonance condition, assuming $g^* = -0.44$ and ideal measurement contrast (from 0.5 to 1). (C) Echo recovery amplitude P_S plotted as a function of $\tau_S - \tau_S'$ for increasing $\tau_S + \tau_S'$ (red points), along with fits to a Gaussian with adjustable height and width. The best-fit width gives $T_2^* = 9$ ns, which is consistent with the value $T_2^* = 10$ ns obtained from singlet decay measurements (Fig. 3B). Best-fit heights (black points) along with the exponential fit to the peak height decay (black curve) give a lower bound on the coherence time T_2 of 1.2 μs.